



CHARACTERIZATION OF SURFACE AND INTERFACE OF Fe-C STEEL UNDER ELECTROLYTIC GALVANIZATION

Ion BIBICU¹, Caius BULEA², Lucian DIAMANDESCU¹, Vasile RUS², Traian POPESCU¹, Ionel MERCIONIU¹

¹National Institute of Materials Physics, Bucharest-Magurele 077125, Romania

²BETAK S.A., Electroplating Department, Bistrita-Nasaud 420063, Romania

Corresponding author: Ion BIBICU,

E-mail: bibicu@infim.ro

Abstract. Low carbon Fe-C steel surface has been studied before and after electrolytic galvanization. The corrosion products formed under atmospheric conditions on the Fe-C steel were identified and characterised by X-ray diffraction (XRD), transmission Mössbauer spectroscopy, conversion electron Mössbauer spectroscopy (CEMS), and conversion X-ray Mössbauer spectroscopy (CXMS). In decreasing order of abundance the found corrosion phases were magnetite, hematite, and goethite. After the surface preparation, an electrolytic galvanization process was applied. A magnetic anisotropy was evidenced after preparation, in the superficial layer of around 250 nm thickness. Scanning electron microscopy (SEM) analyses evidenced the formation of a uniform thin Zn film of 8 μm at the surface of steel. No other Fe-Zn phases were identified at the steel-Zn interface.

Key words: low carbon steel, electrolytic galvanization, Mössbauer effect, X-ray diffraction, scanning electron microscopy.

1. INTRODUCTION

The reduction of corrosion is an important goal of the modern world. The use of Zn coatings is one of the most important anticorrosive protections of steels and has a long history. Galvanization of the steel surface proves protection against atmospheric corrosion for a significant period [1–5]. A variety of galvanizing processes are known: hot-dip galvanizing, galvannealing, electrogalvanizing, and δ -galvanizing [6]. The main industrial process is hot-dip galvanizing that is based on the reaction of liquid zinc with steel and the formation of intermetallic compounds and η -Zinc in coating layer. New researches and development investments are presently in Zn coatings field. These are supported by new sophisticated steels, requirement of strictly controlled microstructure, the lightening of structures with specific surface treatment, the continuous innovation in field of machinery fabrication, and new efficient technologies to obtain thin coatings with high corrosion resistance. Electrogalvanized steel is used increasingly for the manufacture of automobiles, chemical, mechanical, aeronautic, naval, aerospace or military industries, IT, buildings, and other products. Thin and uniform coatings with different structures (composite [7], multilayers, [8, 9], nanostructured [10, 11] etc.) and high corrosion resistance can be obtained by electrodeposition. The great majority of studies are dealing with hot-dip galvanizing.

Relative few studies are dedicated to electrogalvanized process but its number is increasing in the last years. Recent papers assigned to electrogalvanized process show another structure of the Zn coating without Fe-Zn intermetallic compounds presence in deposited layer [12–14]. There are permanent efforts to optimize the existing processes such as the study of electrodeposition conditions [15–17], the effects of additives to electrolyte solutions [18, 19], the effect of organic impurities [20] etc. Also there are studies searching for new alternatives to electrodeposition from aqueous solutions as electrodeposition from ionic liquids [21] and from deep eutectic solvents [22].

In this paper we study the surfaces and interfaces of low carbon Fe-C steel under electrolytic galvanization; the type of deposition: weakly acid electroplating. Low carbon Fe-C steel surface has been

investigated before and after electrolytic galvanization using mainly nondestructive physical techniques. The main corrosion products were identified and the efficiency on the galvanization procedure is highlighted. The obtained information is important from both scientific and technological point of view.

2. EXPERIMENTAL

Chemical composition (in wt%) of steel samples was: carbon 0.04%, manganese 0.37%, silicon 0.009%, phosphorus 0.009%, sulphur 0.008%, aluminium 0.035%, copper 0.03%, chromium 0.02%, nickel 0.01%, titanium 0.001%, and nitrogen 0.005 %. The samples were obtained from hot laminated roll.

The surface preparation was performed on the polishing machine with different grades of emery paper. Water was added intermittently so as to cool down the metal samples. During the grinding operation, the metal samples were rotated at intervals so as to erase previous marks that arose due to the initial grinding. The pickling of the samples was done in diluted HCl acid solution; this was to remove all organic contaminants and oxides, followed by electrolytic degreasing. This was carried out by treating the surface of samples with alkaline solution and subsequent cleaning in water, to remove all grease or oily contaminants.

The electrodeposition of Zn was performed in the standard cell of 267 ml capacity. Chemical reagents used are zinc chloride (75g/l), potassium chloride (220 g/l), and boric acid (23 g/l). All the chemicals were of analytic grade and solutions were prepared using deionized water. The anode of zinc was also immersed to the positive terminal of the rectifier. The current was kept at 1A/dmp for 10 minutes. The immersion depth was kept constant. Finally, the samples were rinsed in water to wash the salt solution off the samples plated, immediately after the electroplating process. The rinsing was done in distilled water then dried in air.

X-ray diffraction (XRD) measurements were carried out at room temperature on a Bruker D8 Advance diffractometer, using CuK_α radiation (1.54051\AA) using standard θ to 2θ geometry. An additional diffractogram was obtained for electrodeposited sample in a detector scan mode. This semi-grazing X-ray diffraction measurement was performed at 5° incidence angle.

Mössbauer effect measurements were performed in two geometries: transmission (TMS) and backscattering. The ^{57}Fe Mössbauer spectra were obtained with a 10 mCi $^{57}\text{Co-Rh}$ source and a conventional constant-acceleration spectrometer (AME-50 Elscint) equipped with CMCA-550 acquisition module. The velocity range was calibrated with $\alpha\text{-Fe}$ standard foil. Lorentzian line shapes were considered to fit the recorded Mössbauer spectra.

All isomer shifts are given relative to that of $\alpha\text{-Fe}$ at room temperature. An absorber from surface of the initial sample was obtained by scrapping. Information about samples surfaces was found in the backscattering geometry by detecting the conversion electrons (CEMS) and the conversion X-rays (CXMS). The electrons penetration depth is of the order of 250 nanometers and the X-rays penetration depth is of the order of 11 microns [μm] [23–25]. The backscattering measurements were conducted at a high degree of accuracy with a new detector, gas-flow proportional [26]. In CXMS measurements, a filter from aluminized mylar with 2.5 microns thickness was used to eliminate the conversion electron signal [27].

The morphology and composition of interface layer were examined using scanning electron microscope (TESCAN LYRA3XMU) with EDX integrated analyzer. Samples were cut to reveal their cross sections with a MTI precision diamond wire saw.

3. RESULTS AND DISCUSSION

3.1. X-RAY DIFFRACTION

The X-ray diffractograms of the investigated samples are shown in Figs. 1 and 2. The Rietveld refinements results are presented in Table 1. The initial sample (Table 1) consists in two prevailing phases – magnetite and hematite accompanied by small goethite phase as a result of corrosion processes. The $\alpha\text{-Fe}$ peak at 45° given by the steel substrate can be also observed. After preparation, the diffractogram of the sample ready for electrodeposition exhibits pure $\alpha\text{-Fe}$ pattern (Fig. 2a). In Fig. 2b the XRD pattern of the electrodeposited sample, displays the peaks of Zn metal as main phase together with a small peak of $\alpha\text{-Fe}$.

The XRD pattern at grazing incidence (Fig. 2c) for the electrodeposited sample exhibits only Zn metal lines and a very small trace (practically buried in the background) of α -Fe.

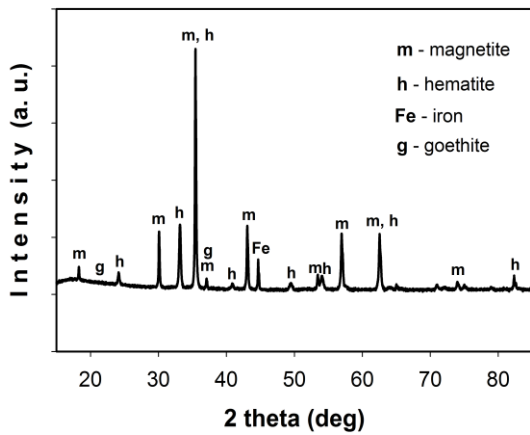


Fig. 1 – The X-ray diffraction pattern on initial sample.

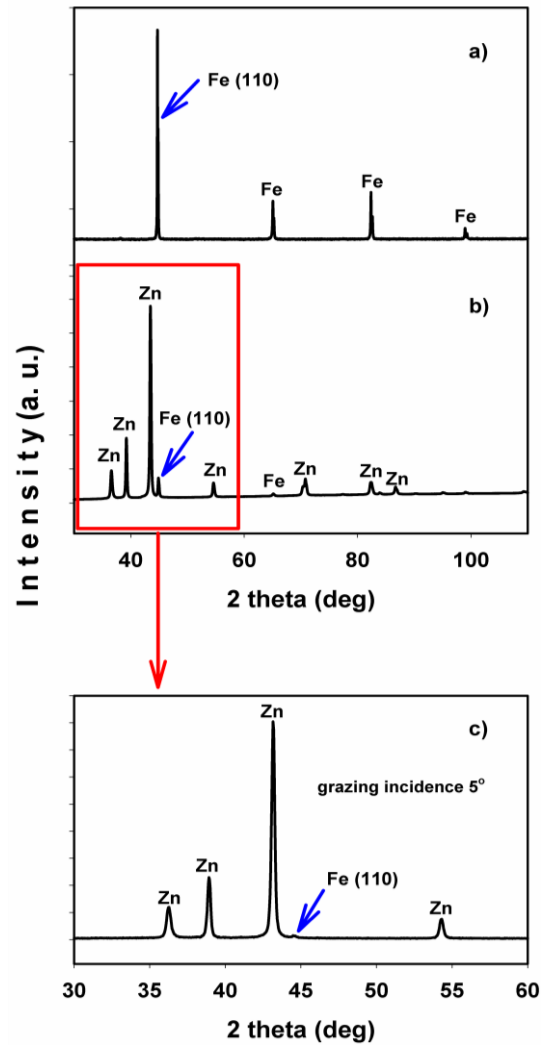


Fig. 2 – The X-ray diffraction patterns on: a) sample ready for electrodeposition; b) electrodeposited sample; c) grazing incidence for electrodeposited sample.

Table 1

Rietveld refinement results on steel samples

Sample	Lattice parameters [Å]			Crystalline Size [nm]	Phase content [wt. %]
	a	b	c		
Initial	8.3963	–	–	>100	Fe ₃ O ₄ 51.0
	5.0540	–	13.7129	>100	α -Fe ₂ O ₃ 44.1
	2.8654	–	–	>100	α -Fe 3.0
	4.6376	9.9392	3.0670	45	α -FeOOH 1.9
Ready for electrodeposition	2.8677	–	–	>100	α -Fe 100
Electrodeposited	2.8688	–	–	>100	α -Fe 5.7
	2.663	–	4.9355	38	Zn 94.3
Errors	±0.0005	±0.0005	±0.0005	±0.5	±0.5

3.2. MÖSSBAUER SPECTROSCOPY

Figures 3–5 show the Mössbauer spectra of the initial sample, the sample ready for deposition and the electrodeposited sample, together with the computer fit (continuous lines). The Mössbauer parameters obtained by fitting the spectra with Lorentzian line shape are given in Table 2.

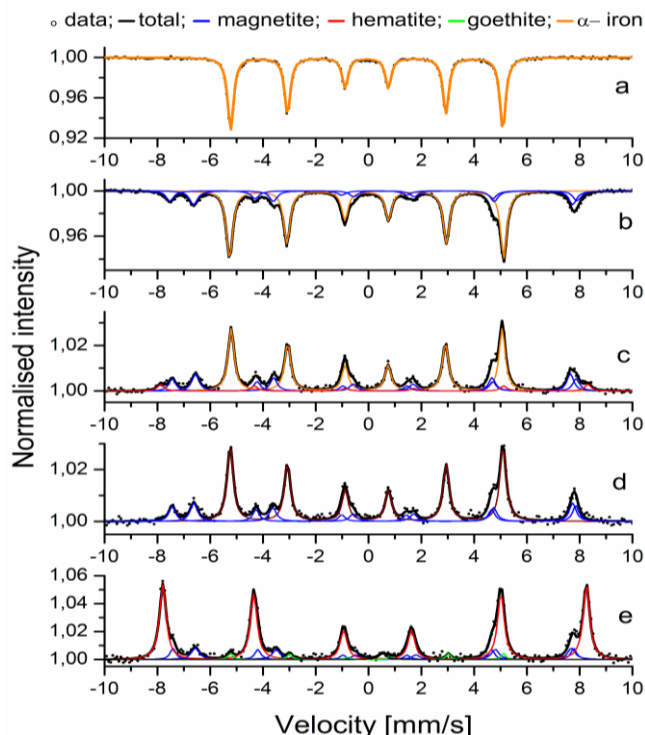


Fig. 3 – Mössbauer spectra of the initial sample:
 a) from bulk; b) of surface scrapped layer; c) by CXMS without filter;
 d) by CXMS with filter; e) by CEMS.

The bulk transmission (Fig. 3a) spectrum was fitted with a single sextet due low carbon content [28, 29]. The line width of the outermost lines confirms the low concentrations of alloying elements.

The surface measurements on initial sample prove a marked corrosion: a coating with a considerable thickness and a complex composition. Hematite is the main compound of the outermost layer (Fig. 3e). Its Mössbauer parameters are practically the same with those given in literature [30–33]. The second compound in the outermost layer is magnetite with a normal stoichiometry as in different references [30, 32, 34]. In the outermost layer there is also goethite. The Mössbauer parameters for goethite have a great dispersion [29, 32, 33, 35]. The reduced hyperfine magnetic field of goethite compared with well-crystallized goethite (around 380 kOe), can be generally assigned to varying crystallinity of goethite and/or small particles. Poor crystallinity and substitution may modify the spectrum of goethite to such an extent that characterization must be carried out at low temperatures [30]. According to the level diagram of Gibbs free energies of formation for some corrosion products of iron, α -FeOOH is a level in the transition to α -Fe₂O₃ [36]. Also a corrosion product can exist in the outermost layer at sensibility limit of the method. Its presence is suggested by smoothing the spectrum. CEMS spectra indicate a corrosion layer thickness greater than 250 nm. The spectrum of steel substrate was not evidenced.

The surface spectra obtained by CXMS without electron filter (Fig. 3c) give the integral information about superficial corrosion layer. The magnetite and hematite are the compounds of the layer. Magnetite is now the main compound of the corrosion layer. The using of the electron filter hides the hematite presence (Fig. 3d). Also the hematite is not present in the surface sample collected by scape method (Fig. 3b). The data obtained for sample collected by scape method are very closely to those obtained by CXMS with electron filter. All CXMS spectra evidenced the steel substrate.

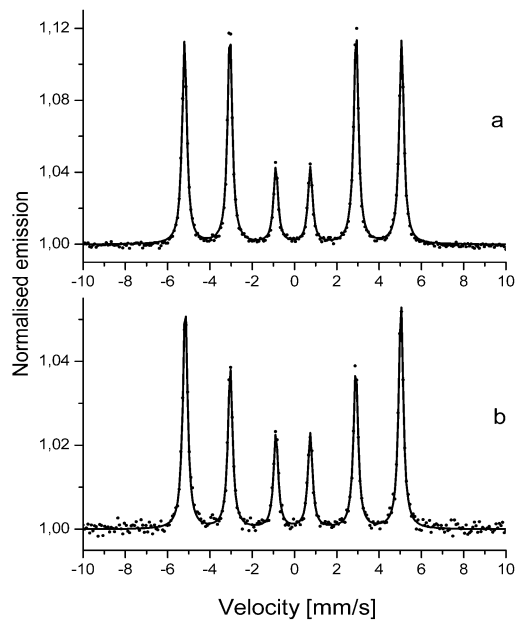


Fig. 4 – Mössbauer spectra of the sample ready for electrodeposition: a) by CEMS; b) by CXMS without filter.

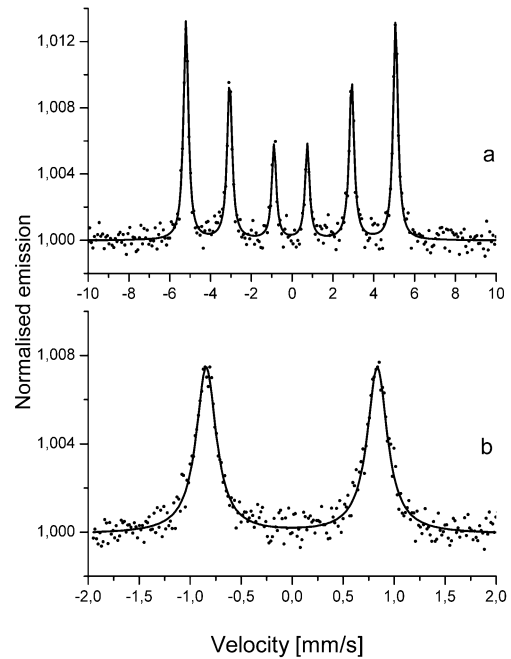


Fig. 5 – Mössbauer spectra by CXMS of the electrodeposited sample: a) at high velocity range; b) at low velocity range.

The results of all Mössbauer measurements show the presence of a corrosion layer on initial steel sample. The layer compounds are magnetite, hematite, and goethite. The relative concentration in increasing order is: goethite, hematite, and magnetite. The goethite and hematite are located at the surface of corrosion layer. We estimate the corrosion layer thickness around 5 microns.

The spectra of the samples ready for electrodeposition (Fig. 4) show the moving off the corrosion layer and the presence of α -Fe. The Fe sextet has hyperfine parameters, practically the same as for the initial sample. The intensities of the second and fifth peaks of these sextets with respect to the third and fourth peaks, in CEMS spectra (Fig. 4a), showed that the directions of the γ -ray and magnetic moments were nearly perpendicular and thus indicate a magnetic anisotropy at surface samples [28, 37, 38]. The magnetic moments of iron tend to be orientated in surface plane. By contrast, the TMS and CXMS showed that the magnetic moments inside the sample were in a random arrangement. The anisotropy found in superficial layer of around 250 nm thickness, by CEMS spectra, is obtained, mainly, due to the preparation process of steel sheets for galvanization.

The CXMS spectra of the electrodeposited sample (Fig. 5), obtained for two velocity ranges, evidenced properly steel substratum and its parameters are practically the same as those obtained before deposition. The spectra did not show the presence of a new intermetallic compound between steel and Zn coating. The spectrum obtained at lower velocity range and greater statistics was used for better detection of possible compounds from interface layer steel – Zn coating; compounds possibly similar to those found in hot-dip galvanizing [39] or reported in Ref. [40].

Table 2

Mössbauer parameters of the studied samples from fitted spectrum, taken at 300 K, where H: magnetic hyperfine field at ^{57}Fe nucleus; IS: isomer shift relative to α -Fe; QS: quadrupole splitting

Sample	Geometry	H [kOe]	IS [mm/s]	QS [mm/s]	Line Width [mm/s]	Relative Content [%]	Assignment
Initial samples for electrolytic galvanization							
Volume sample	TMS	331.4	0.00	0.01	0.28	100.00	Alpha-Fe
Collected surface	TMS	333.9	0.00	0.00	0.30	69.80	Alpha-Fe
		464.6	0.67	-0.01	0.37	17.24	Magnetite-site I
		499.7	0.28	-0.01	0.38	12.96	Magnetite-site II

Table 2
(continued)

Sample	Geometry	H [kOe]	IS [mm/s]	QS [mm/s]	Line Width [mm/s]	Relative Content [%]	Assignment
Surface without electron filter	CXMS	332.0	0.00	0.01	0.29	61.43	Alpha-Fe
		461.2	0.64	0.02	0.32	18.69	Magnetite-site I
		497.6	0.32	-0.02	0.32	13.08	Magnetite-site II
		524.8	0.40	-0.18	0.31	6.80	Hematite
Surface with electron filter	CXMS	333.4	0.00	0.00	0.29	67.23	Alpha-Fe
		461.2	0.66	0.02	0.33	18.23	Magnetite-site I
		497.6	0.29	0.01	0.30	14.43	Magnetite-site II
Surface	CEMS	462.9	0.71	-0.07	0.36	12.55	Magnetite-site I
		493.6	0.30	-0.04	0.28	9.32	Magnetite-site II
		522.3	0.37	-0.20	0.32	72.67	Hematite
		334.4	0.30	0.18	0.26	4.12	Goethite
		-	0.45	-	0.54	1.34	Corrosion product
Samples ready for electrolytic galvanization							
Surface without filter	CXMS	331.2	0.01	0.01	0.27	100.00	Alpha-Fe
Surface	CEMS	330.1	0.00	0.01	0.27	100.00	Alpha-Fe
Samples after electrolytic galvanization							
Surface without filter	CXMS	331.3	0.00	0.01	0.29	100.00	Alpha-Fe
Surface without filter; lower velocity	CXMS	-	0.00	1.68	0.25	100.00	Alpha-Fe
Errors		±3	±0.02	±0.04	±0.03	±1.5	

3.3. SCANNING ELECTRON MICROSCOPY

The SEM cross sectional image (Fig. 6) of Zn coating shows that the thickness of the coating is around 8 microns. The Zn coating form a continuous and uniform layer proved by EDS analysis. For the Zn deposition, the dispersion is quite uniform. Qualitative EDS analysis (Fig. 7) established the essential composition with Fe and Zn being the major constituents.

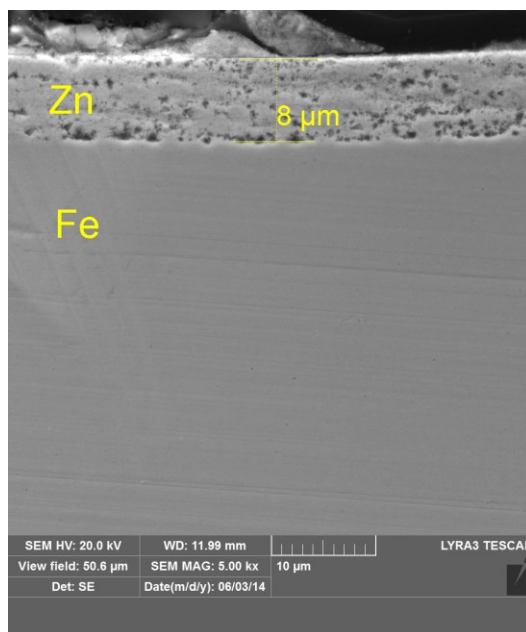


Fig. 6 – SEM cross section image of Zn–Fe electrodeposited coating.

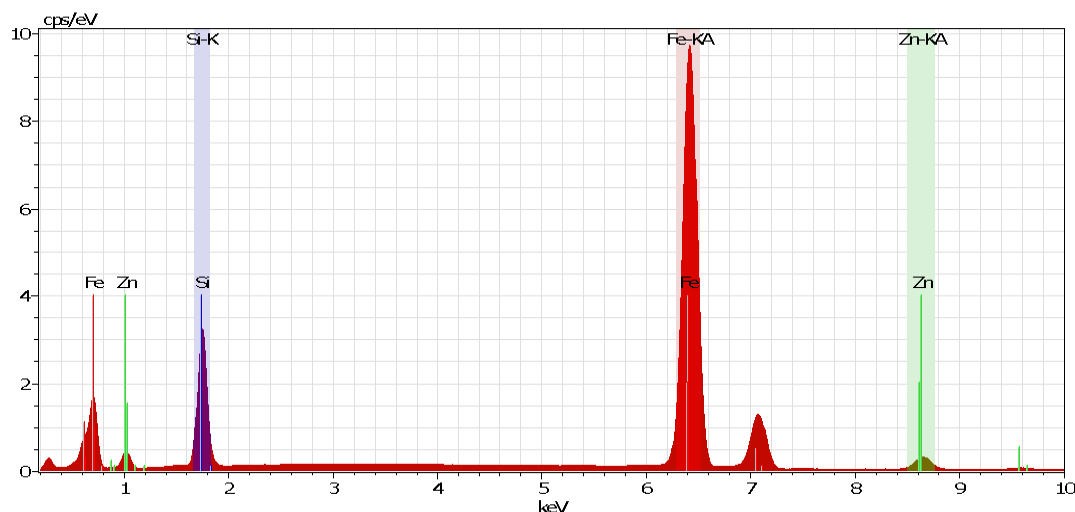


Fig. 7 – EDS of Zn-Fe interface.

4. CONCLUSIONS

The Fe-C steel surface has been studied before and after electrolytic galvanization, mainly by XRD and combined Mössbauer spectroscopy. On the initial Fe-C steel sample, corroded under atmospheric conditions, the identified corrosion products were (in concentration decreasing order): magnetite, hematite, and goethite. The goethite and hematite are located at the surface of corrosion layer. The preparation process removed the corrosion layer and a magnetic anisotropy was found in the superficial layer of 250 nm thickness. The Zn layer was found to be uniform, with 8 μm thickness. No intermetallic compounds were identified at the Zn-steel interface.

ACKNOWLEDGMENTS

Financial support from the National Authority for Scientific Research (ANCS) (Core Program contract PN09-45) is gratefully acknowledged.

REFERENCES

1. J. MACKOWIAK, N.R. SHORT, *Metallurgy of galvanised coatings*, Int. Met. Rev., **24**, pp. 1–19, 1979.
2. O. KUBASCHEWSKI, *Iron-Binary Phase Diagrams*, Springer-Verlag, Berlin Heidelberg, 1982,
3. Y. DE ABREU, A. DA SILVA, A. RUIZ, A. RÉQUIZ, N. ANGULO, R. ALANIS, *Study of zinc coatings on steel substrate attained by two different techniques*, Surf. Coat. Techn., **120–121**, pp. 682–688, 1999.
4. A.R. MARDER, *The metallurgy of zinc coated steel*, Prog. Mat. Sci., **45**, pp. 191–271, 2000.
5. K. BAI, P. WU, *Assessment of Zn-Fe-Al system for kinetic study of galvanizing*, J. Alloys Comp., **347**, pp. 156–164, 2002.
6. O. UWAAKWEH, A. JORDAN, *Application of metastable transformation of mechanically alloyed Fe-Zn in equilibrium phase studies*, Journal of Phase Equilibria, **18**, 5, pp. 448–457, 1997.
7. A.P.I. POPOOLA, O.S.I. FAYOMI, V.S. AIGBODION, M. ABDULWABAB, *Surface modification, strengthening effect and electrochemical study of Zn-Al₂O₃-CeO₃ and Zn-TiO₂-CeO₃ coating on mild steel*, Int. J. Adv. Manuf. Technol., **85**, pp. 1419–1427, 2016.
8. S. RASHMI, L. ELIAS, A.C. Hegde, *Multilayered Zn-Ni alloy coatings for better corrosion protection of mild steel*, Engineering Science and Technology-An International Journal-Jestech, **20**, 3, pp. 1227–1232, 2017.
9. B. BAHADORMANESH, M. GHORBANI, *Electrodeposition of Zn-Ni-P compositionally modulated multilayer coatings: An attempt to deposit Ni-P and Zn-Ni alloys from a single bath*, Electrochemistry Communications, **81**, pp. 93–96, 2017.
10. A. VLASA, S. VARVARA, A. POP, C. BULEA, L.M. MURESAN, *Zn-TiO₂ nanocomposite coatings with improved corrosion behavior obtained by electrolytic codeposition*, J. Appl. Electrochem., **40**, 8, pp. 1519–1527, 2010.
11. Y. SALHI, S. CHERROUL, M. CHERKAoui, K. ABDELOUANDI, *Electrodeposition of nanostructured Sn-Zn coatings*, Applied Surface Science, **367**, pp. 64–69, 2016.

12. S. BASAVANNA, Y. ARTHOBA NAIK, *Electrochemical studies of Zn–Ni alloy coatings from acid chloride bath*, J. Appl. Electrochem., **39**, pp. 1975–1982, 2009.
13. A.P.I. POPOOLA, O.S.I. FAYOMI, O.M. POPOOLA, *Comparative studies of microstructural tribological and corrosion properties of plated Zn and Zn-alloy coatings*, Int. J. Electrochem. Sci., **7**, pp. 4860–4870, 2012.
14. O.S.I. FAYOMI, A.P.I. POPOOLA, *An investigation of the properties of Zn coated mild steel*, Int. J. Electrochem. Sci., **7**, pp. 6555–6570, 2012.
15. P.I. NEMES, M. LEKKA, L. FEDRIZZI, L.M. MURESAN, *Influence of the electrodeposition current regime on the corrosion resistance of Zn–CeO₂ nanocomposite coatings*, Surface and Coatings Technology, **252**, pp. 102–107, 2014.
16. N.P. WASEKAR, A. JYOTHIRMAYI, N.HEBALKAR, G. SUNDARARAJAN, *Influence of pulsed current on the aqueous corrosion resistance of electrodeposited zinc*, Surface & Coatings Technology, **272**, pp. 373–379, 2015.
17. N.D. NIKOLIC, P.M. ZIVKOVIC, G. BRANKOVIC, M.G. PAVLOVIC, *Estimation of the exchange current density and comparative analysis of morphology of electrochemically produced lead and zinc deposits*, Journal of the Serbian Chemical Society, **82**, 5, pp. 539–550, 2017.
18. K. MIYAZAKI, A. NAKATA, Y.S. LEE, T. FUKUTSUKA, T. ABE, *Influence of surfactants as additives to electrolyte solutions on zinc electrodeposition and potential oscillation behaviour*, Journal of Applied Electrochemistry, **46**, 10, pp. 1067–1073, 2016.
19. L. YUAN, ZY. DING, SJ. LIU, WF. SHU, YN. HE, *Effects of additives on zinc electrodeposition from alkaline zincate solution*, Transactions of Nonferrous Metals Society of China, **27**, 7, pp. 1656–1664, 2017.
20. D. MAJUSTE, F.C. BUBANI, R.E. BOLMARO, E.L.C. MARTINS, P.R. CETLIN, V.S.T. CIMINELLI, *Effect of organic impurities on the morphology and crystallographic texture of zinc electrodeposits*, Hydrometallurgy, **169**, pp. 330–338, 2017.
21. F.M. RIVAS-ESQUIVEL, G.M. BRISARD, R. ORTEGA-BORGES, G. Y. TREJO, *Meas. Zinc Electrochemical Deposition from Ionic Liquids and Aqueous Solutions Onto indium tin*, International Journal of Electrochemical Science, **12**, 3, pp. 2026–2041, 2017.
22. N.M. PEREIRA, C.M. PEREIRA, J.P. ARAUJO, A.F. SILVA, *Zinc electrodeposition from deep eutectic solvent containing organic additives*, Journal of Electroanalytical Chemistry, **801**, pp. 545–551, 2017.
23. J.R. GANCEDO, M. GARCIA, J.F. MARCO, J.A. TABARES, *Corrosion studies by CEMS. Facing the experiment*, Hyperfine Interact., **111**, pp. 83–92, 1998.
24. I. BIBICU, *Mossbauer spectroscopy applied to surface study*, Revue Roumaine de Chimie, **57**, 9–10, pp. 877–889, 2012.
25. I. BIBICU, S. CONSTANTINESCU, D. TARABASANU-MIHAILA, M.N. GRECU, *CEMS measurements on low ⁵⁷Fe doped anatase nanoparticles*, Romanian Reports in Physics, **68**, 4, pp. 1506–1512, 2016.
26. I. BIBICU, G. NICOLESCU, C. CRETU, *A versatile gas-flow proportional counter for Mössbauer spectroscopy*, Hyperfine Interact., **192**, pp. 85–91, 2009.
27. LAURA K. PERRY, D.H. RYAN, R. GAGNON, *Studying surfaces and thin films using Mössbauer spectroscopy*, Hyperfine Interact., **170**, pp. 131–143, 2006.
28. I. BIBICU, A. SAMIDE, M. PREDA, *Steel corrosion in diluted ammoniac solutions studied by Mössbauer spectrometry*, Materials Letters, **58**, pp. 2650–2653, 2004.
29. E. GÜLER, *Phase transitions in a high-chromium and medium-carbon steel*, Materials Chemistry and Physics, **107**, pp. 183–185, 2008.
30. R.M. CORNELL, U. SCHWERTMANN U., *The iron oxides: structure, properties, reactions, occurrences and uses*, second edition, Wiley-VCH Verlag GmbH&Co. KGaA, Weinheim, 2003.
31. A. KUNO, M. MATSUO, A. PASCUAL SOTO, K. TSUKAMOTO, *Mössbauer spectroscopic study of a mural painting from Morgadal Grande, Mexico*, Hyperfine Interact., **156/157**, pp. 431–437, 2004.
32. E. MURAD, *The characterization of soils, clays, and clay firing products*, Hyperfine Interact., **111**, pp. 251–259, 1998.
33. B.F.O. COSTA, M. BLUMERS, A. SANSANO, G. KLINGELHOFER, F. RULL, R. LEHMANN, F. RENZ, *Klimt artwork: material investigation by backscattering Fe-57 Mössbauer and Raman spectroscopy*, Hyperfine Interact., **226**, pp. 621–627, 2014.
34. F.B. WAANDERS, A.F. MULABA-BAFUBIANDI, L. LODYA, *The South African industry use of Mössbauer spectroscopy to solve operational problems*, Hyperfine Interact., **226**, pp. 721–735, 2014.
35. S. MUSIC, S. POPOVIC, *Mossbauer spectroscopic and X-ray diffraction study of the thermal decomposition of natural siderite and goethite*, Journal of Radioanalytical and Nuclear Chemistry, **111**, 1, pp. 27–41, 1987.
36. W. MEISEL, *Degradation of materials and passivity*, Hyperfine Interact., **111**, pp. 59–70, 1998.
37. W. OLSZEWSKI, K. SZYMANŃSKI, D. SATUŁA, L. DOBRZYŃSKI, L. BOTTYÁN, F. TANCZIKÓ, *Magnetic texture determination by conversion electron Mössbauer spectroscopy with circularly polarized beam*, Nuclear Instruments and Methods in Physics Research B, **266**, pp. 3319–3324, 2008.
38. W. KEUNE, *Application of Mössbauer spectroscopy in magnetism*, Hyperfine Interact., **204**, pp. 13–45, 2012.
39. D.C. COOK, *Applications of Mössbauer spectroscopy in industry*, Hyperfine Interact., **141/142**, pp. 21–34, 2002.
40. Y. LI, S. LI, Y. XU, W. WU, P. AURIC, *Layered structure of Fe-Zn electrodepositions*, Hyperfine Interact., **69**, pp. 577–580, 1991.